Stanford Exploration Project, Report 77, November 17, 1997, pages 1–116

Stanford Exploration Project, Report 77, November 17, 1997, pages 1–116

Amplitude and phase in DMO and MZO algorithms

Alexander M. Popovici[1]

keywords: *DMO, prestack, amplitudes, Fourier transform, NMO*

ABSTRACT

In constant velocity, the sequence Dip Moveout (DMO), Normal Moveout (NMO), Stacking and Zero-Offset Migration (ZOM) is equivalent to Prestack Migration. In this context the Dip-Moveout correction can be expressed in two ways. First, DMO can be defined kinematically in time-space domain and implemented in Fourier domain (Hale 1983). Second, DMO can be defined as a process separated out of Prestack Migration, after eliminating the NMO, Stacking and ZOM steps. I simplify the comparison between the two methods by incorporating the sequence DMO, NMO and Stacking into a single process named Migration to Zero-Offset (MZO). MZO is a kinematic process than can be implemented in a manner similar to Hale's and Zhang's DMO, by adding the NMO step as a time shift in the Fourier domain. Second, I define MZO as the process separated out of Prestack Migration, after eliminating the Zero-Offset Migration step. I compare the amplitude and phase output of the two MZO algorithms together with Hale's and Zhang's DMO algorithms for three simple models. The results suggest that the two methods are not equivalent.

INTRODUCTION

The Dip Moveout correction (DMO) is usually defined from geometric or kinematic analysis. Given the ray-theoretic definition of the operator, there is a certain amount of disagreement between researchers as what a "true amplitude operator" should be.

Deregowski and Rocca (1981) define migration to zero-offset (DMO+NMO) as the sequence of prestack migration followed by zero-offset modeling. Following this definition an impulse in a prestack constant-offset section is transformed into a depth model that represents all the possible reflector locations (an ellipse in constant velocity). By modeling the reflector back to zero-offset one obtains a curve that represents the impulse response of the MZO operator. The impulse response curve can be applied to constant-offset data as a Kirchhoff integral operator. The authors also define

[1]**email:** not available

the amplitude along the DMO operator as being proportional to the curvature of the operator. Black et al. (1993) address the problem of the "true amplitude operator" by requiring the amplitude along the DMO operator to preserve the reflectivity of a dipping reflector. The DMO amplitudes found in time-space domain coincide with Zhang's (1988) modification of the original Hale Fourier domain DMO.

Hale (1983) has a ray-theoretical definition of DMO. However in the third chapter of his thesis he tries to reconcile the kinematic definition with a wave-equation approach. He starts with the prestack migration equation and isolates fours processing steps: NMO, DMO, stacking and zero-offset migration. The problem can be simplified by dissecting prestack migration into only two processing steps: migration to zero-offset and zero-offset migration. This simplification avoids the subtle flaw that Hale has in his derivation, which leads to an inaccurate analytical expression for DMO.

By including the NMO correction in the Fourier domain Zhang DMO, I obtain an MZO processing step which I compare with the MZO as obtained from the prestack migration dissection. The MZO obtained from prestack migration performs NMO, DMO and stacking in one step. I apply the two different MZO methods to three simple prestack synthetic models and compare the amplitude and phase of the output. The results suggest the two methods are not equivalent.

First definition: MZO by Fourier transform

Both Hale and Zhang separate the NMO correction from the DMO correction. However for variable velocity media this can not be done, and in order to generalize the NMO $\cdot$ DMO operation the migration to zero-offset (MZO) concept has to be used. Migration to zero-offset is the process that transforms a nonzero-offset (constant offset) section into a zero-offset section. In constant velocity media MZO = NMO+DMO.

Taking into account the geometry in Figure **??** the MZO correction in constant velocity media is

$$\begin{cases} \Delta y_0 = \dfrac{2h^2 \sin\theta}{v\sqrt{t_h^2 - 4h^2 \frac{\cos^2\theta}{v^2}}} \\[2ex] t_0 = \dfrac{t_h^2 - \frac{4h^2}{v^2}}{\sqrt{t_h^2 - 4h^2 \frac{\cos^2\theta}{v^2}}}, \end{cases} \tag{1}$$

where h is the half offset, t_0 is twice the zero-offset travel time from the reflection point to the surface, v is the velocity of the medium and t_h is the constant-offset travel time.

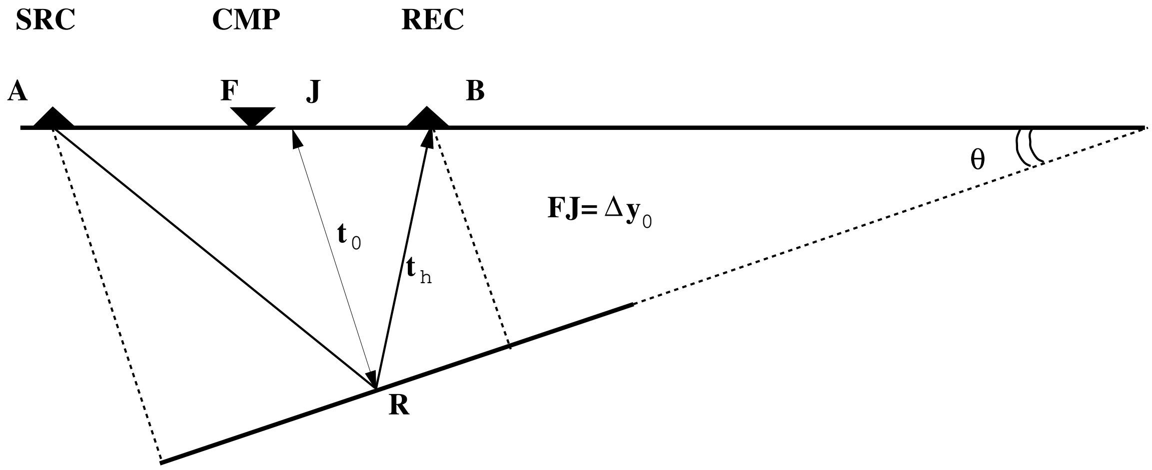

Figure 1: Geometry for a dipping reflector in a constant velocity medium. The zero-offset ray **JR** and the nonzero-offset ray bounce at the same reflection point **R**. The dipping angle is θ. mihai2-MZOdip [NR]

The MZO correction for a given dip θ is

$$\begin{cases} y_0 = y - \dfrac{2h^2 \sin\theta}{v\sqrt{t_h^2 - \frac{4h^2}{v^2} + 4h^2 \frac{\sin^2\theta}{v^2}}} \\ \\ t_0 = \dfrac{t_h^2 - \frac{4h^2}{v^2}}{\sqrt{t_h^2 - \frac{4h^2}{v^2} + 4h^2 \frac{\sin^2\theta}{v^2}}}. \end{cases} \tag{2}$$

To clarify the sign convention for the spatial coordinate in equation (2), we can notice that the y-axis is oriented to the left, and the angles are positive if the reflector dips toward the right and negative if the reflector dips toward the left. In Figure **??** the angle θ is negative. This can be also derived from the equation

$$\frac{dt_0}{dy_0} = \frac{2\sin\theta}{v} = \frac{k_{y_0}}{\omega_0}$$

where the sign of dy_0 determines the sign of the angle θ.

The differentials of the new variables are

$$\begin{cases} dy_0 = dy \\ \\ dt_0 = \dfrac{t_h(t_h^2 - \frac{4h^2}{v^2} + 2h^2 \frac{k_{y_0}^2}{\omega_0^2})}{(t_h^2 - \frac{4h^2}{v^2} + h^2 \frac{k_{y_0}^2}{\omega_0^2})^{\frac{3}{2}}} dt_h \end{cases} \tag{3}$$

The 2-D Fourier transform of the zero-offset field is

$$P_0(\omega_0, k_{y_0}, h) = \int_{t_0} dt_0 \int_{y_0} dy_0 \, e^{i(\omega_0 t_0 - k_{y_0} y_0)} p_0(t_0, y_0, h). \tag{4}$$

Following Hale's (1984) technique, replace the variables t_0 and y_0 in equation (4) with their expression in equation (2). Fortunately, it is not necessary to express explicitly $t_h = t_h(t_0, y_0)$ and $y = y(t_0, y_0)$, though the respective dependencies are assumed.

After replacing the variables y_0 and t_0 in equation (4), the migration to zero-offset transformation becomes

$$\begin{aligned} P_0(\omega_0, k_{y_0}, h) &= \int dt_h \int dy \frac{t_h(t_h^2 - \frac{4h^2}{v^2} + 2h^2\frac{k_{y_0}^2}{\omega_0^2})}{(t_h^2 - \frac{4h^2}{v^2} + h^2\frac{k_{y_0}^2}{\omega_0^2})^{\frac{3}{2}}} p(t_h, y, h)\, e^{i(\omega_0\sqrt{t_h^2 - \frac{4h^2}{v^2} + h^2\frac{k_{y_0}^2}{\omega_0^2}} - k_{y_0}y)} \\ &= \int dt_h \frac{t_h(t_h^2 - \frac{4h^2}{v^2} + 2h^2\frac{k_{y_0}^2}{\omega_0^2})}{(t_h^2 - \frac{4h^2}{v^2} + h^2\frac{k_{y_0}^2}{\omega_0^2})^{\frac{3}{2}}} p(t_h, k_{y_0}, h)\, e^{i\omega_0\sqrt{t_h^2 - \frac{4h^2}{v^2} + h^2\frac{k_{y_0}^2}{\omega_0^2}}} \end{aligned} \tag{5}$$

Note that by replacing the quantity

$$t_h^2 - \frac{4h^2}{v^2} = t_n^2$$

in equation (5), we get the same phase as the one obtained by Hale and Zhang, but the Jacobian differs from Zhang's Jacobian by a factor

$$\frac{J_M}{J_Z} = \frac{t_h}{t_n} = \sqrt{1 + \frac{4h^2}{v^2 t_n^2}}, \tag{6}$$

which corresponds to the Jacobian of the NMO transformation.

Second definition: MZO extracted from prestack migration

Hale (1984) starts with the prestack migration equation in common-midpoint and offset coordinates and tries to isolate four major processing steps. The four steps are

1. DMO,
2. NMO,
3. Stacking,
4. Zero-offset migration.

By considering steps 1, 2, and 3 as a single process (MZO), I isolate only two steps:

- Migration to zero-offset.
- Zero-offset migration.

After extracting the zero-offset migration from the prestack migration equation, we are left with the migration to zero-offset operator.

For a constant velocity, downward continue the field $p(t,h,y,z=0)$ recorded at the surface, to a depth $z=\Delta z$

$$p(\omega,k_h,k_y,z=\Delta z) = e^{ik_z(\omega,k_h,k_y)\Delta z} p(\omega,k_h,k_y,z=0) \tag{7}$$

for all values of ω, k_h, k_y. The prestack migration imaging step consists of summing for all the values of ω and k_h after downward continuation. To image for $t=0$ and $h=0$:

$$p(t=0,h=0,k_y,z) = \int d\omega \int dk_h \; e^{ik_z(\omega,k_h,k_y)z} p(\omega,k_h,k_y,z=0) \tag{8}$$

where k_z is given by

$$k_z(\omega,k_h,k_y) \equiv -\frac{\omega}{v}\left\{\left[1-\frac{v^2}{4\omega^2}(k_y+k_h)^2\right]^{\frac{1}{2}} + \left[1-\frac{v^2}{4\omega^2}(k_y-k_h)^2\right]^{\frac{1}{2}}\right\}. \tag{9}$$

Following Hale's (1984) derivation, introduce a new variable ω_0 in order to isolate the zero-offset migration operator. The substitution is based on the equation

$$\omega \equiv \omega_0\left[1+\frac{v^2k_h^2}{4\omega_0^2-v^2k_y^2}\right]^{\frac{1}{2}}. \tag{10}$$

Substituting ω in equation (9) the downward continuation operator $k_z(\omega,k_h,k_y)$ is transformed into

$$k_z \equiv -\frac{2\omega_0}{v}\left[1-\frac{v^2k_y^2}{4\omega_0^2}\right]^{\frac{1}{2}} \tag{11}$$

The downward continuation operator now has the same form as the one for zero-offset. In order to isolate the zero-offset migration operator, the variable ω_0 is substituted for ω and then the order of integration is changed between ω_0 and k_h. The integration boundaries have to be observed carefully.

Integration limits

From now on for simplicity I will use the variables

$$v_h = \frac{vk_h}{2}$$

$$v_y = \frac{vk_y}{2}.$$

In equation (8), the values of the constant k_z have to be real. Imaginary values of k_z do not satisfy the downward continuation ordinary differential equation:

$$\frac{\partial^2 P}{\partial z^2} = -k_z^2 P \tag{12}$$

and have to be excluded. Real values of k_z from equation (9) require both of the following conditions to be satisfied:

$$\begin{cases} \mid \omega \mid & \geq & \mid v_y + v_h \mid \\ \mid \omega \mid & \geq & \mid v_y - v_h \mid \end{cases}$$

which can be reduced to the condition

$$\mid \omega \mid \quad \geq \quad \mid v_y \mid + \mid v_h \mid \tag{13}$$

Therefore, equation (8) should be written

$$\begin{aligned} p(t=0, h=0, k_y, z) \quad = \quad & \int_{-\infty}^{\infty} dk_h \int_{-\infty}^{-(|v_h|+|v_y|)} d\omega e^{ik_z(\omega,k_h,k_y)z} p(\omega, k_h, k_y, z=0) \\ + \quad & \int_{-\infty}^{\infty} dk_h \int_{|v_h|+|v_y|}^{\infty} d\omega e^{ik_z(\omega,k_h,k_y)z} p(\omega, k_h, k_y, z=0) \end{aligned} \tag{14}$$

For each value of v_y the integration in ω is done in two regions: under the value $\omega = -(\mid v_h \mid + \mid v_y \mid)$ and over the value $\omega = (\mid v_h \mid + \mid v_y \mid)$ as displayed in Figure **??**.

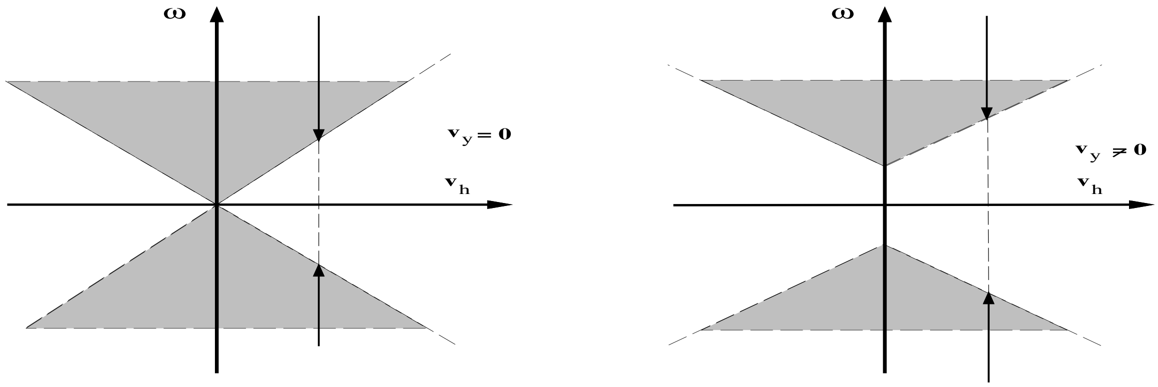

Figure 2: Regions of integration. $\boxed{\text{mihai2-khkyomega}}$ [NR]

Before substituting the new variable ω_0 in the prestack migration equation let us analyze the limits of integration for the new variable ω_0. From Appendix A, the expression of $\omega_0(\omega, k_h, k_y)$ is

$$\omega_0^2 = \frac{1}{2}\left[\omega^2 + v_y^2 - v_h^2 + \sqrt{(\omega^2 + v_y^2 - v_h^2)^2 - 4\omega^2 v_y^2}\right] \tag{15}$$

and the boundary values for ω_0 corresponding to the limits for ω in equation (13):

$$\mid \omega_0 \mid \quad \geq \quad \sqrt{v_y^2 + \mid v_y v_h \mid} \; .$$

Integration order

By taking equation (14) and changing the integration variable from ω to ω_0. In the same time the new variable $k_z(\omega, k_h, k_y)$ becomes function of only two variables in $k_z(\omega_0, k_y)$, in the form given by equation (11).

$$
\begin{aligned}
p(t=0, h=0, k_y, z) &= \int_{-\infty}^{\infty} dk_h \int_{-\infty}^{-(|v_h|+|v_y|)} d\omega e^{ik_z(\omega,k_h,k_y)z} p(\omega, k_h, k_y, z=0) \\
&+ \int_{-\infty}^{\infty} dk_h \int_{|v_h|+|v_y|}^{\infty} d\omega e^{ik_z(\omega,k_h,k_y)z} p(\omega, k_h, k_y, z=0) \\
&= \int_{-\infty}^{\infty} dk_h \int_{-\infty}^{-\sqrt{v_y^2+|v_y v_h|}} d\omega_0 \left[\frac{d\omega}{d\omega_0}\right] e^{ik_z(\omega_0,k_y)z} p^*(\omega_0, k_h, k_y, z=0) \\
&+ \int_{-\infty}^{\infty} dk_h \int_{\sqrt{v_y^2+|v_y v_h|}}^{\infty} d\omega_0 \left[\frac{d\omega}{d\omega_0}\right] e^{ik_z(\omega_0,k_y)z} p^*(\omega_0, k_h, k_y, z=0).
\end{aligned} \tag{16}
$$

Special attention should be given to the new field $p^*(\omega_0, k_h, k_y, z=0)$. As the variable ω is replaced with ω_0, each value of ω_0 has to be associated with the appropriate value of the field

$$
p(\omega, k_h, k_y, z=0) = p(\omega = \omega_0 \sqrt{1 + \frac{v_h^2}{\omega_0^2 - v_y^2}}, k_h, k_y, z=0).
$$

The new field $p^*(\omega_0, k_h, k_y, z=0)$ represents a remapping (or interpolation) of the original field $p(\omega, k_h, k_y, z=0)$. Each value in the new field $p^*(\omega_0, k_h, k_y, z=0)$ with coordinates (ω_0, k_h, k_y) corresponds to the value in the field $p(\omega, k_h, k_y, z=0)$ with coordinates $(\omega = \omega_0\sqrt{1 + \frac{v_h^2}{\omega_0^2 - v_y^2}}, k_h, k_y)$. A more detailed analysis of this mapping is done in a companion paper in this report: Popovici (1993).

From equation (10) the Jacobian is

$$
J = \left[\frac{d\omega}{d\omega_0}\right] = (1 + \frac{v_h^2}{\omega_0^2 - v_y^2})^{-\frac{1}{2}} \left[1 - \frac{v_h^2 v_y^2}{(\omega_0^2 - v_y^2)^2}\right]. \tag{17}
$$

In the next step we change the integration order

$$
\begin{aligned}
p(t=0,h=0,k_y=0,z) &= \int_{-\infty}^{\infty} dk_h \int_{-\infty}^{-\sqrt{v_y^2+|v_y v_h|}} d\omega_0 J e^{ik_z(\omega_0,k_y)z} p^*(\omega_0,k_h,k_y,z=0) \\
&+ \int_{-\infty}^{\infty} dk_h \int_{\sqrt{v_y^2+|v_y v_h|}}^{\infty} d\omega_0 J e^{ik_z(\omega_0,k_y)z} p^*(\omega_0,k_h,k_y,z=0) \\
&= \int_{-\infty}^{\infty} d\omega_0 e^{ik_z(\omega_0,k_y)z} \int_{\frac{2(-\omega_0^2+v_y^2)}{v|v_y|}}^{\frac{2(\omega_0^2-v_y^2)}{v|v_y|}} dk_h J p^*(\omega_0,k_h,k_y,z=0) \\
&= \int_{-\infty}^{\infty} d\omega_0 e^{ik_z(\omega_0,k_y)z} p_0(\omega_0,k_y)
\end{aligned}
\tag{18}
$$

where $p_0(\omega_0, k_y)$ is defined as

$$
p_0(\omega_0,k_y) = \int_{\frac{2(-\omega_0^2+v_y^2)}{v|v_y|}}^{\frac{2(\omega_0^2-v_y^2)}{v|v_y|}} dk_h J p^*(\omega_0,k_h,k_y,z=0) \tag{19}
$$

Equation (18) represents zero-offset downward continuation and imaging as introduced by Gazdag (1978) or Stolt (1978). Equation (19) represents a way of obtaining zero-offset section from constant-offset sections.

The operations needed to obtain the zero-offset stacked section from the constant-offset field described in equation (19) are:

1. Fourier transform the constant-offset field $p_h(t,h,y) \rightarrow p_h(\omega,k_h,k_y)$.
2. Remap (interpolate) the ω axis into ω_0.
3. Multiply by the Jacobian.
4. Integrate over k_h.
5. Inverse Fourier transform $p_0(\omega_0,k_y) \rightarrow p_0(t_0,y)$.

Comparing the amplitudes of the methods

I can not compare impulse responses in constant offset sections because the MZO extracted from prestack migration includes an integration over the offset variable. The reason why I cannot just inverse Fourier transform in offset coordinates is explained in detail in the companion paper (Popovici, 1993). On short, the remapping of the field $p_h(\omega,k_h,k_y) \rightarrow p_h^*(\omega_0,k_h,k_y)$ performs implicitly a summation over the offset. Therefore I compare the stacked output of the MZO in Fourier domain (applied to each constant offset section) and the output of the MZO extracted from prestack-migration applied to the whole prestack data cube. I will call the MZO defined in Fourier domain: FT-MZO, and the MZO extracted from prestack migration: Ps-MZO.

The first model is a diffractor situated at a depth of 600 meters. The velocity used is 2000 m/s and the number of offsets is 64. The maximum half-offset h is 1575 meters. The modeling was done by calculating the travel-time from source to diffractor and back to receiver, and assigning to each midpoint an amplitude equal to the product

$$Amp = \frac{1}{t_{src}} \frac{1}{t_{rec}},$$

where t_{src} is the travel-time from source to the diffractor and t_{rec} is the travel-time from the diffractor to the receiver. The NMO applied to the constant-offset sections prior to processing via Hale's or Zhang's DMO has a Jacobian equal to

$$J_{NMO} = \frac{t_{src} + t_{rec}}{t_{NMO}}.$$

I compare the results obtained with and without applying the spherical divergence correction. Figure **??** shows the first and last panel in the prestack data cube corresponding to the zero-offset and the maximum-offset common-midpoint (CMP) sections. Figure **??** shows the output of the two MZO algorithms. Figure **??**a shows the FT-MZO after stacking all independent offsets and Figure **??**b shows the output of applying Ps-MZO to the entire prestack data cube. While in both cases the kinematics are the same, the maximum amplitudes along the zero-offset hyperbola shown in Figure **??**a show there are significant differences between the two algorithms. The highest amplitude curve in Figure **??**a belongs to the Ps-MZO section, followed by the original zero-offset model, Zhang's DMO, Hale's DMO and FT-MZO. I expected the FT-MZO to follow exactly Zhang's curve as it actually happens for the dipping reflector in Figure **??** where the two curves practically coincide. Figure **??**b shows results obtained when applying the spherical divergence correction. Figure **??** compares the wavelets obtained after MZO. For each method I selected the trace passing through the CMP above the diffractor. Figure **??**b has spherical divergence applied. As Hale's DMO curve always follows Zhang's DMO curve but at a lower amplitude, I removed this curve from the next comparisons, in an attempt to unclutter the figures.

The second model represents a dipping reflector through a medium with 2000 m/s velocity. Figure **??** shows the first and last panel in the prestack data cube corresponding to the zero-offset and the maximum-offset common-midpoint (CMP) sections. The model was produced by considering the dipping reflector comprised of diffractors, each modeled separately. Figure **??**a shows the output of the stacked FT-MZO, while Figure **??**b shows the output of the Ps-MZO algorithm. Figure **??** shows the amplitudes along the dipping reflector. This is the case where Zhang's amplitude curve is superimposed on the FT-MZO curve as I expected from theory. Figure **??**b shows results obtained when applying the spherical divergence correction. The values at the sides of the figure should be discarded as the picking algorithm I used to collect the amplitudes along the reflector, chose the amplitudes along the artifacts generated by spatial wraparound. Figure **??** compares the wavelets obtained after MZO. For each method I selected the trace passing through the middle of the section. Again Figure **??**b has spherical divergence applied. Observe that in both cases the FT-DMO follows the zero-offset original curve, while the phase of the Ps-MZO wavelet is very different.

The third model represent a horizontal reflector through a medium with 2000 m/s velocity. Figure **??** shows the first and last panel in the prestack data cube corresponding to the zero-offset and the maximum-offset common-midpoint (CMP) sections. Figure **??**a shows the output of the stacked FT-MZO, while Figure **??**b shows the output of the Ps-MZO algorithm. Figure **??** shows the amplitudes along the horizontal reflector. Figure **??**b shows results obtained when applying the spherical divergence correction. Again the maximum amplitude corresponds to the Ps-MZO, followed by Zhang's DMO, original zero-offset model and FT-MZO. When spherical divergence is applied all three methods show amplitudes higher than the original model. Figure **??** compares the wavelets obtained after MZO. For each method I selected the trace passing through the middle of the section. Again Figure **??**b has spherical divergence applied. While the two FT-MZO wavelets follow closely the zero-offset original model, the phase of the Ps-MZO wavelet is less similar.

I don't have a good explanation yet for the difference in amplitudes between Zhang's DMO and FT-MZO in the case of the single diffractor and in the case of the horizontal reflector. A loss in amplitude in the FT-MZO methods, occurs due to stacking, as the amplitude of the zero-offset sections after DMO tend to decrease slightly with the offset. This could be due to my modeling or to the fact that the DMO Jacobian doesn't completely account for the loss in amplitude with offset. In think the spherical divergence correction should be part of the DMO process and not an independent process, as it should be dip dependent.

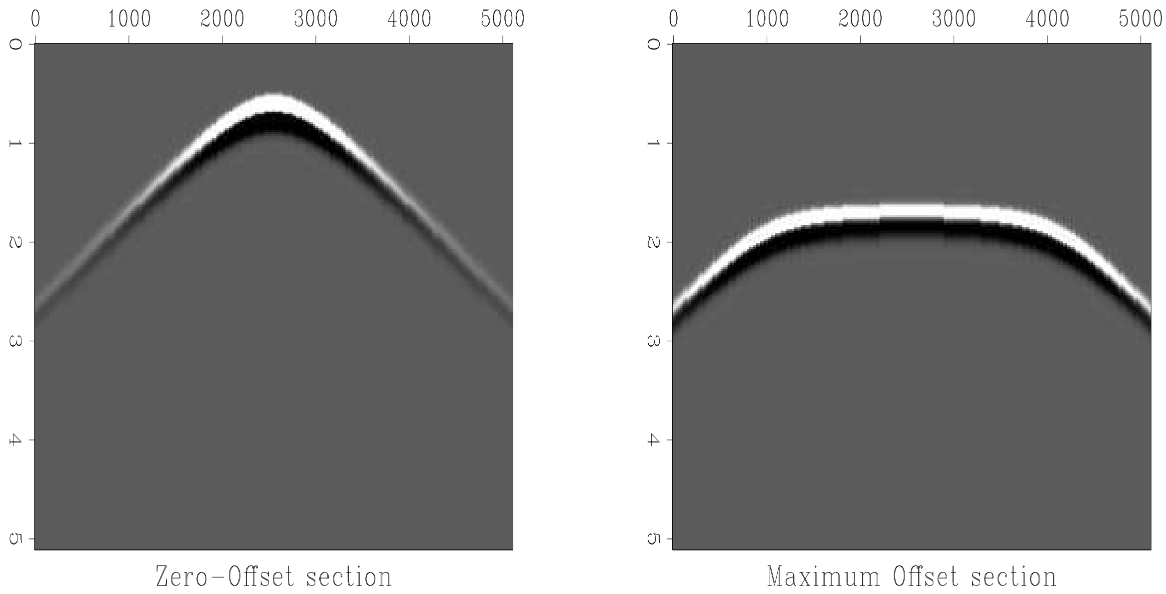

Figure 3: Input to the DMO and MZO algorithms.
a. First panel in the input cube: zero-offset.
b. Last panel in the input cube: maximum-offset. mihai2-coFig1 [ER]

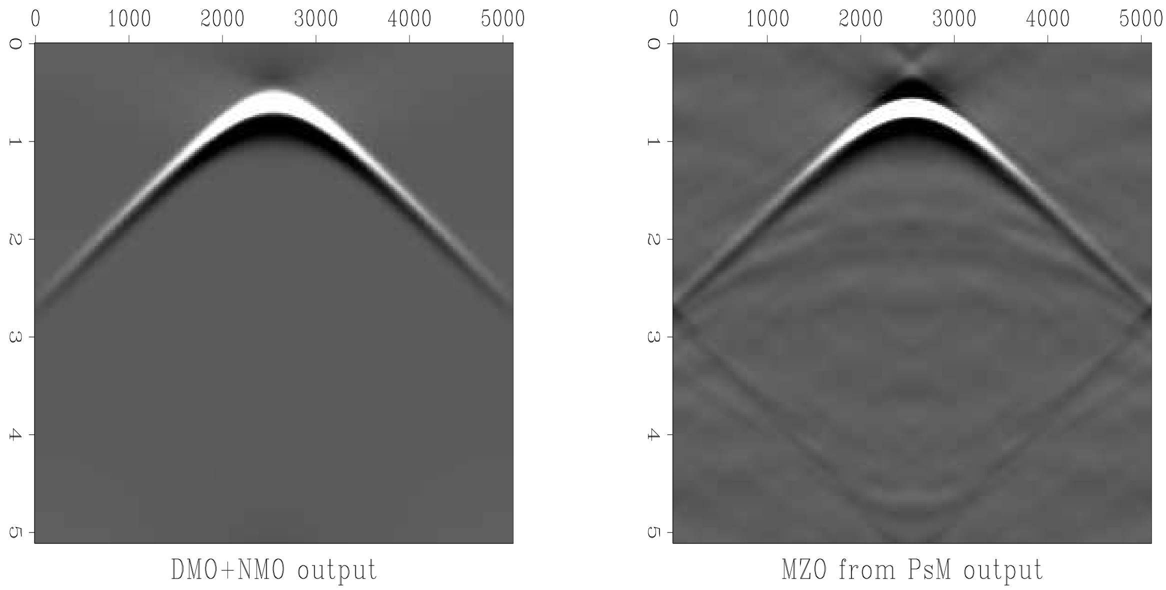

Figure 4: Output of the DMO and MZO algorithms.
a. DMO+NMO.
b. MZO from Prestack Migration. mihai2-zoFig1 [CR]

CONCLUSIONS

I compare the results of MZO applied via two different methods. The Fourier domain MZO is obtained by including the NMO step to Zhang's DMO as a phase shift in Fourier domain. The MZO extracted from prestack migration is obtained by separating the prestack double square root equation into a zero-offset migration step and a migration to zero-offset step. By applying the two types of MZO to three simple synthetic models I conclude that the two definitions are not equivalent.

REFERENCES

Biondi, B., and Ronen, J., 1987, Dip moveout in shot profiles: Geophysics, **52**, 1473–1482.

Black, J.L., Schleicher, K.L., and Zhang, L., 1993, True-amplitude imaging and dip moveout: Geophysics, **58**, 47–66.

Deregowski, S. M., and Rocca, F., 1981, Geometrical optics and wave theory of constant-offset sections in layered media: Geophysical Prospecting, **29**, 374–406.

Jakubowitz, H., 1990, A simple efficient method of dip-moveout correction: Geophysical Prospecting, **38**, 221-245.

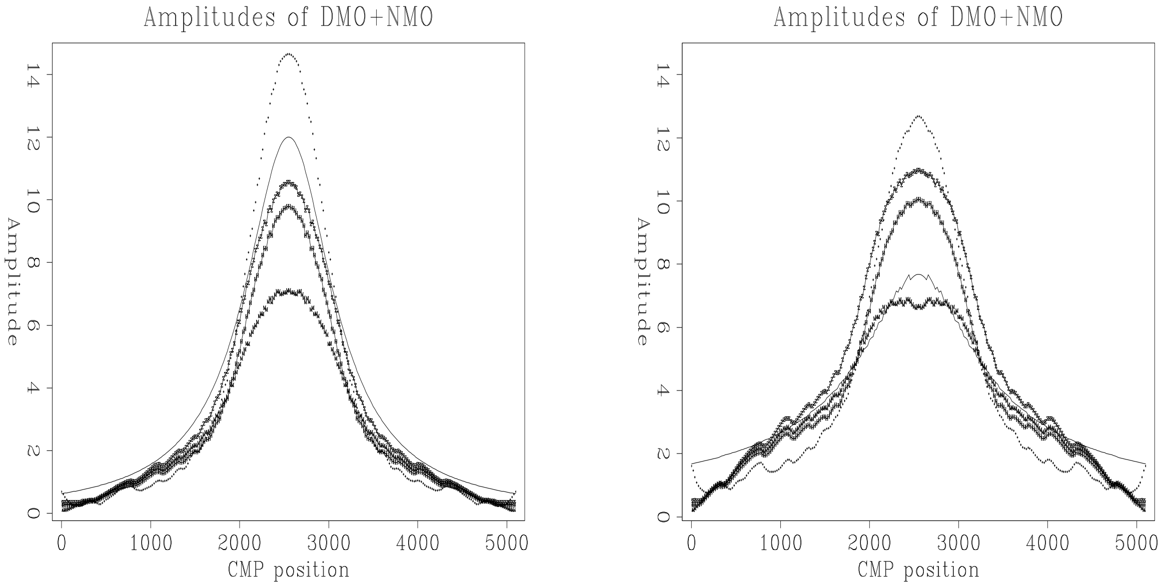

Figure 5: a. Amplitudes along the zero-offset hyperbola. **H**-line: DMO via Hale after NMO. **Z**-line: Zhang DMO. **M**-line: MZO (DMO+NMO) in Fourier domain. Dotted-line: MZO from Prestack Migration. Continuous line: amplitudes along original zero-offset hyperbola.
b. Amplitudes with spherical divergence applied. **H**-line: DMO via Hale after NMO. **Z**-line: Zhang DMO. **M**-line: MZO (DMO+NMO) in Fourier domain. Dotted-line: MZO from Prestack Migration. Continuous line: amplitudes along original zero-offset hyperbola. mihai2-ampDMO1 [CR]

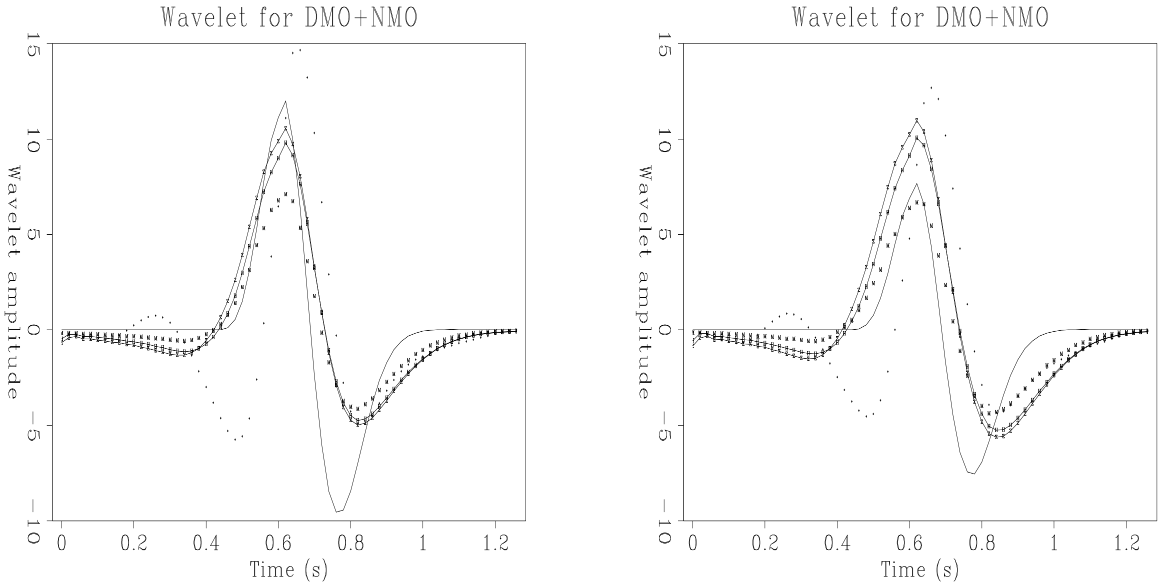

Figure 6: a. Zero-offset wavelets through top of hyperbola. **H**-line: Hale. **Z**-line: Zhang. **M**-line: MZO by FT. Dotted-line: MZO from PsM. Continuous line: original wavelet.
b. Zero-offset wavelets with spherical divergence applied. **H**-line: Hale. **Z**-line: Zhang. **M**-line: MZO by FT. Dotted-line: MZO from PsM. Continuous line: original wavelet. mihai2-wavDMO1 [CR]

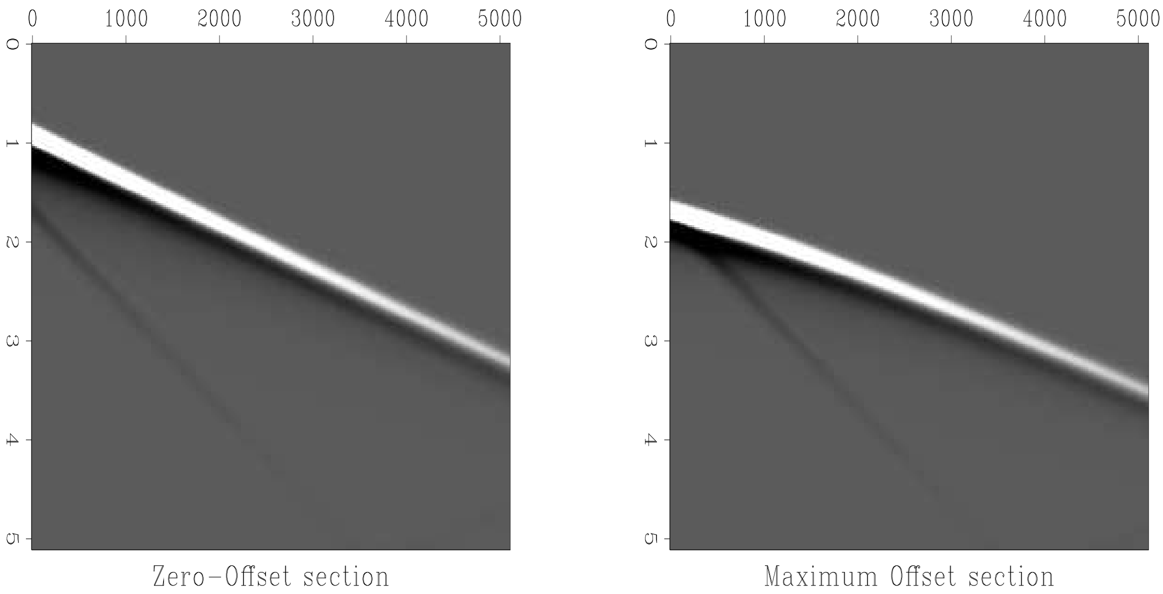

Figure 7: Input to the DMO and MZO algorithms.
a. First panel in the input cube: zero-offset.
b. Last panel in the input cube: maximum-offset. mihai2-coFig2 [ER]

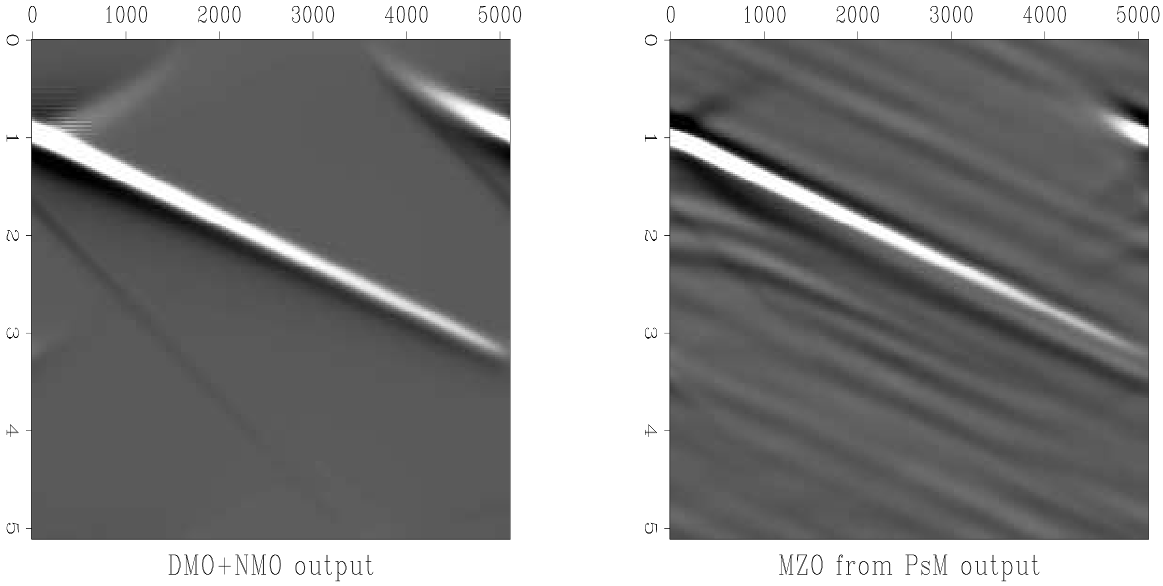

Figure 8: Output of the DMO and MZO algorithms.
a. DMO+NMO.
b. MZO from Prestack Migration. mihai2-zoFig2 [CR]

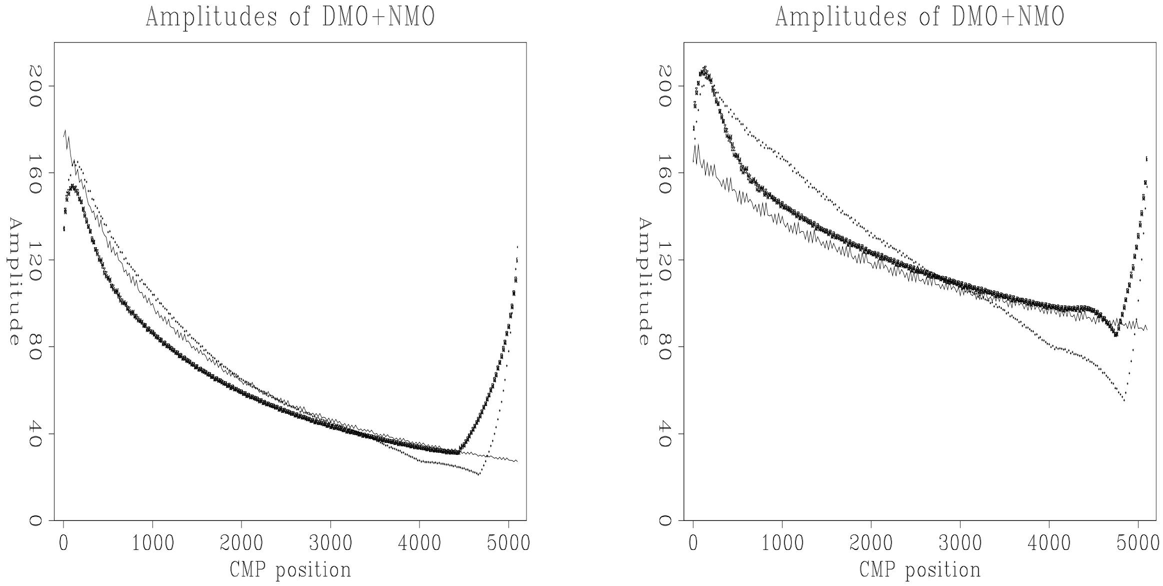

Figure 9:
a. Amplitudes along a dipping reflector. **Z**-line: DMO via Zhang after NMO. **M**-line: MZO (DMO+NMO) in Fourier domain. Dotted-line: MZO from Prestack Migration. Continuous line: amplitudes along original zero-offset reflector.
b. Amplitudes with spherical divergence applied. **Z**-line: DMO via Zhang after DMO. **M**-line: MZO (DMO+NMO) in Fourier domain. Dotted-line: MZO from Prestack Migration. Continuous line: amplitudes along original zero-offset reflector. mihai2-ampDMO2 [CR]

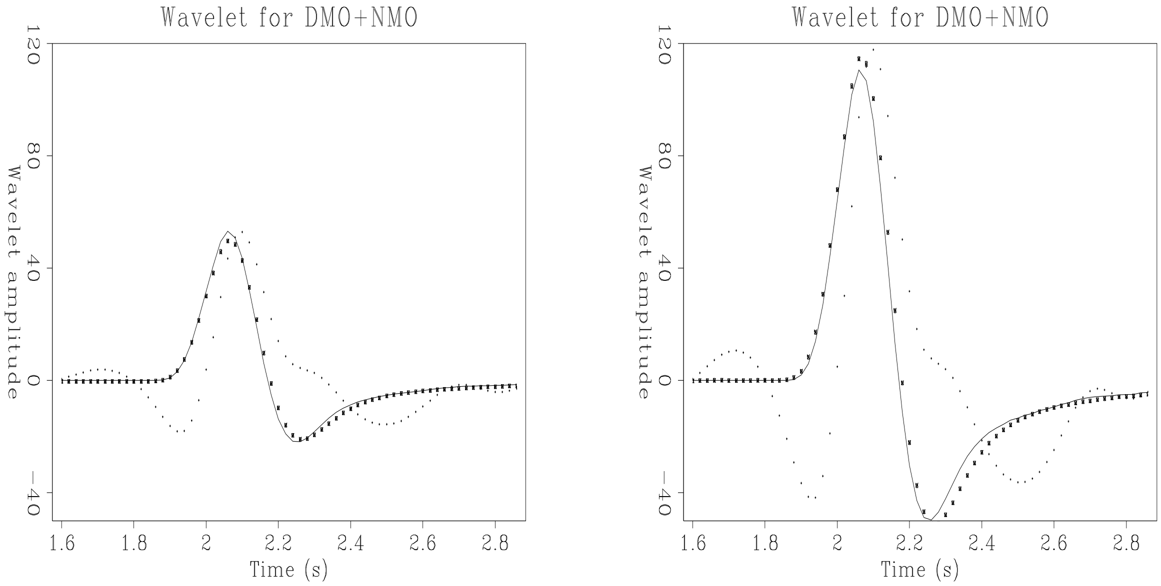

Figure 10:
a. Zero-offset wavelets. **Z**-line: Zhang. **M**-line: MZO by FT. Dotted-line: MZO from PsM. Continuous line: original wavelet.
b. Zero-offset wavelets with spherical divergence applied. **Z**-line: Zhang. **M**-line: MZO by FT. Dotted-line: MZO from PsM. Continuous line: original wavelet. mihai2-wavDMO2 [CR]

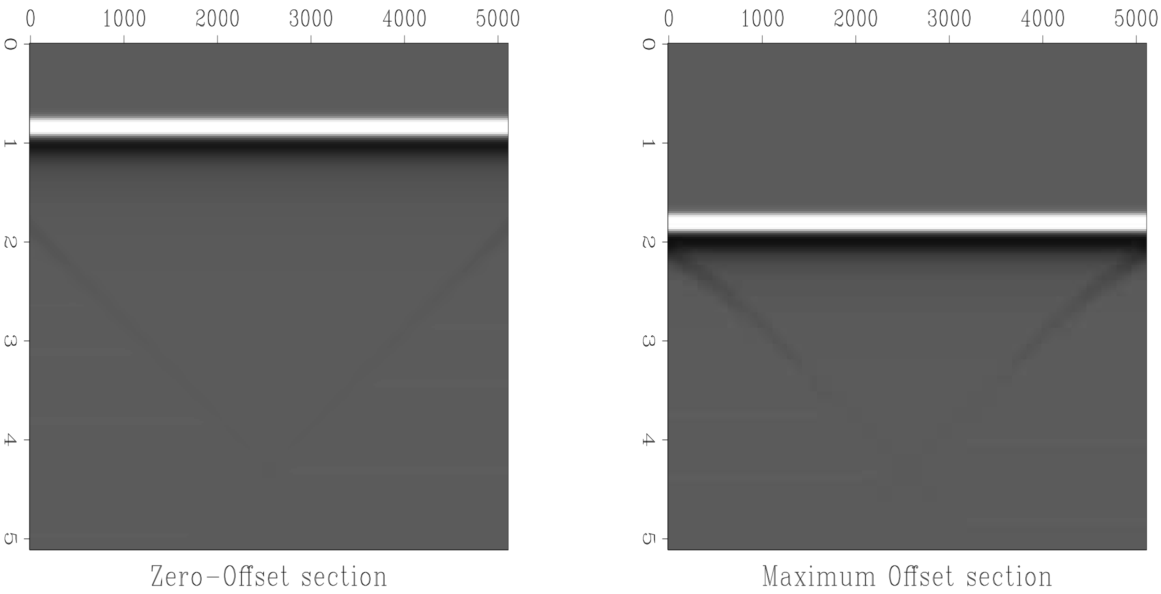

Figure 11: Input to the DMO and MZO algorithms.
a. First panel in the input cube: zero-offset.
b. Last panel in the input cube: maximum-offset. mihai2-coFig3 [ER]

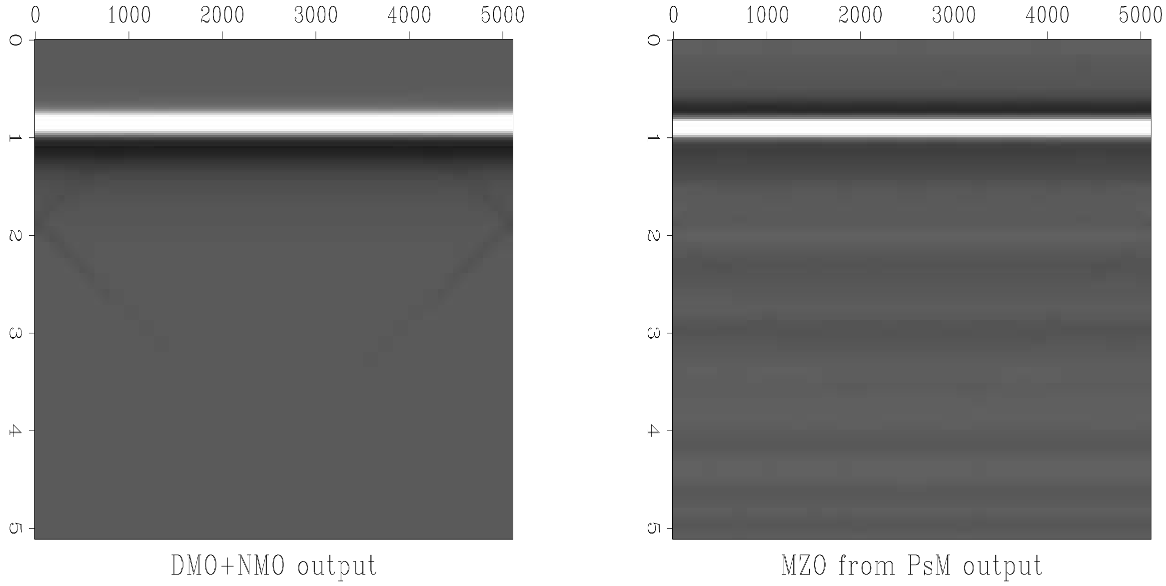

Figure 12: Output of the DMO and MZO algorithms.
a. DMO+NMO.
b. MZO from Prestack Migration. mihai2-zoFig3 [CR]

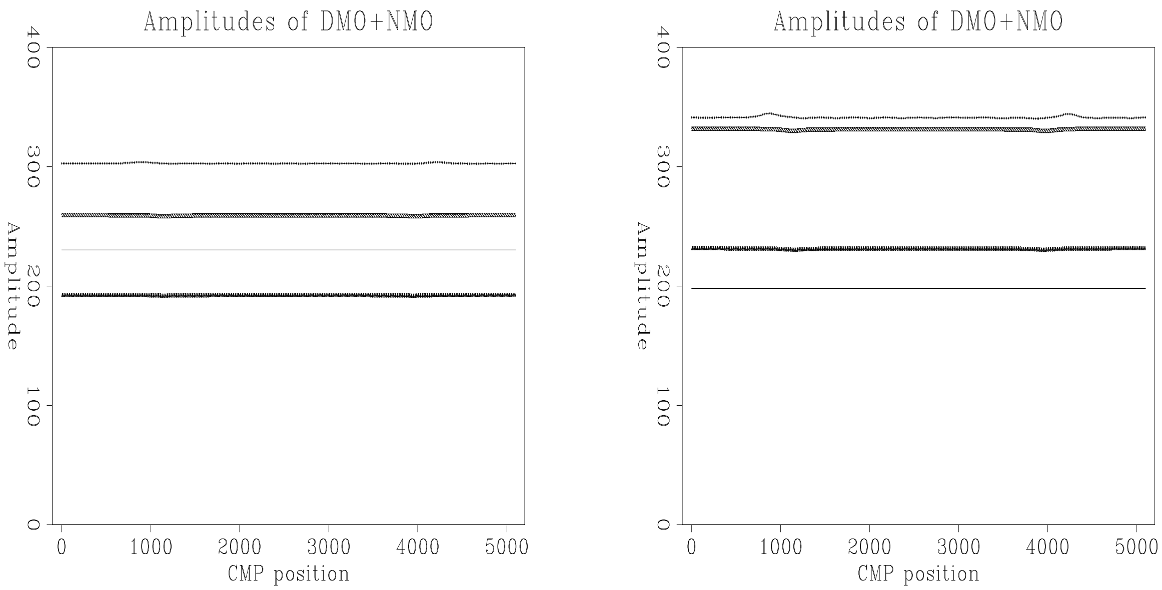

Figure 13:
a. Amplitudes along a horizontal reflector. **Z**-line: DMO via Zhang after NMO. **M**-line: MZO (DMO+NMO) in Fourier domain. Dotted-line: MZO from Prestack Migration. Continuous line: amplitudes along original zero-offset reflector.
b. Amplitudes with spherical divergence applied. **Z**-line: DMO via Zhang after DMO. **M**-line: MZO (DMO+NMO) in Fourier domain. Dotted-line: MZO from Prestack Migration. Continuous line: amplitudes along original zero-offset reflector. mihai2-ampDMO3 [CR]

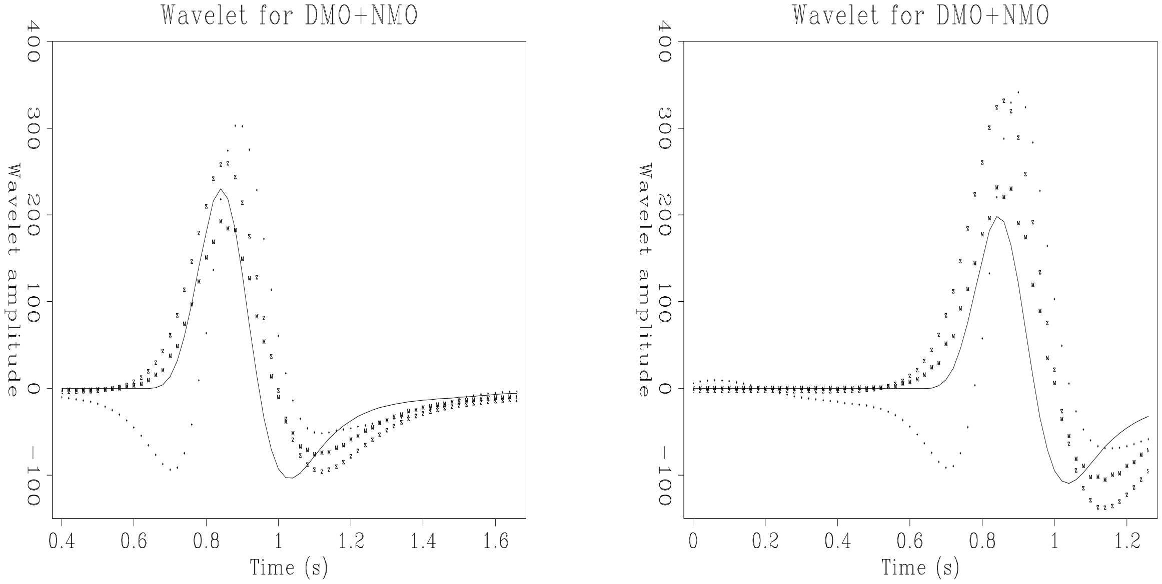

Figure 14:
a. Zero-offset wavelets. **Z**-line: Zhang. **M**-line: MZO by FT. Dotted-line: MZO from PsM. Continuous line: original wavelet.
b. Zero-offset wavelets with spherical divergence applied. **Z**-line: Zhang. **M**-line: MZO by FT. Dotted-line: MZO from PsM. Continuous line: original wavelet. mihai2-wavDMO3 [CR]

Hale, I. D., 1983, Dip-moveout by Fourier transform: Ph.D. thesis, Stanford University.

Popovici, A.M., 1993, Partial Differential Equation for Migration to Zero-Offset: SEP–**77**, 77–88.

Yilmaz, O., and Claerbout, J. F., 1980, Prestack partial migration: Geophysics, **45**, 1753-1779.

Zhang, L., 1988, A new Jacobian for dip moveout: SEP–**59**, 201–208.

APPENDIX A

The purpose of this appendix is to express $\omega_0 = \omega_0(\omega, k_y, k_h)$ and to find the integration limits for ω_0 given the integration limits for ω. Start with the expression for ω:

$$\omega^2 = \omega_0^2 + \frac{\omega_0^2 v_h^2}{\omega_0^2 - v_y^2} \tag{A-1}$$

and after reducing

$$\omega^2\omega_0^2 - \omega^2 v_y^2 = \omega_0^4 - \omega_0^2 v_y^2 + \omega_0^2 v_h^2$$

and grouping

$$\omega_0^4 - \omega_0^2(\omega^2 + v_y^2 - v_h^2) + \omega^2 v_y^2 = 0$$

we have

$$\omega_0^2 = \frac{1}{2}(\omega^2 + v_y^2 - v_h^2 \pm \sqrt{(\omega^2 + v_y^2 - v_h^2)^2 - 4\omega^2 v_y^2}) \qquad \text{(A-2)}$$

The discriminant Δ is

$$\Delta = (\omega - v_y - v_h)(\omega - v_y + v_h)(\omega + v_y - v_h)(\omega + v_y + v_h).$$

From the conditions on k_z in equation (12), Δ is always positive and therefore ω_0^2 is real.

The integration limits for ω_0 are found by starting with the limits ω :

$$\omega = \mid v_h \mid + \mid v_y \mid$$

and after we square both sides

$$\omega^2 = v_h^2 + v_y^2 + 2 \mid v_h v_h \mid$$

and replacing ω^2 in the equation for ω_0^2 we have

$$\begin{aligned}
\omega_0^2 &= \frac{1}{2}\left[v_h^2 + v_y^2 + 2 \mid v_h v_y \mid + v_y^2 - v_h^2 + \sqrt{(2v_y^2 + 2 \mid v_h v_y \mid)^2 - 4v_y^2(v_h^2 + v_y^2 + 2 \mid v_h v_y \mid)}\right] \\
&= \frac{1}{2}\left[2v_y^2 + 2 \mid v_h v_y \mid + \sqrt{4v_y^4 + 4v_h^2 v_y^2 + 8v_y^2 \mid v_h v_y \mid - 4v_y^2 v_h^2 - 4v_y^4 - 8v_y^2 \mid v_h v_y \mid}\right] \\
&= v_y^2 + \mid v_h v_y \mid .
\end{aligned} \qquad \text{(A-3)}$$